Title

Numerical investigation reveals challenges in measuring the contrast recovery coefficients in PET

Journal

Physics in Medicine and Biology, 68(21)

ISSN

0031-9155

Authors

Bayerlein, Reimund

Spencer, Benjamin A

Abdelhafez, Yasser G

et al.

Publication Date

2023-11-07

DOI

10.1088/1361-6560/ad00fa

Peer reviewed

HHS Public Access

Author manuscript

Phys Med Biol. Author manuscript; available in PMC 2024 October 26.

Published in final edited form as:

Phys Med Biol. ; 68(21): . doi:10.1088/1361-6560/ad00fa.

Numerical investigation reveals challenges in measuring the contrast recovery coefficients for PET

Reimund Bayerlein[1], **Benjamin A Spencer**[1], **Yasser G Abdelhafez**[1,2], **Simon R Cherry**[3,1], **Ramsey D Badawi**[1,3], **Negar Omidvari**[3]

[1]Department of Radiology, University of California Davis, Davis, CA, USA.

[2]Radiotherapy and Nuclear Medicine Department, South Egypt Cancer Institute, Assiut University, Egypt.

[3]Department of Biomedical Engineering, University of California Davis, Davis, CA, USA.

Abstract

Objective.—Contrast recovery coefficient (CRC) is essential for image quality (IQ) assessment in positron emission tomography (PET), typically measured according to the NEMA NU 2 standard. This study quantifies systematic uncertainties of the CRC measurement by a numerical investigation of the effects from scanner-independent parameters like voxel size, region-of-interest (ROI) misplacement, and sphere position on the underlying image grid.

Approach.—CRC measurements with 2D and 3D ROIs were performed on computer-generated images of a NEMA IQ-like phantom, using voxel sizes of 1–4 mm for sphere diameters of 5–40 mm – first in absence of noise and blurring, then with simulated spatial resolution and image noise with varying noise levels. The systematic uncertainties of the CRC measurement were quantified from above variations of scanner-independent parameters. Subsampled experimental images of a NEMA IQ phantom were additionally used to investigate the impact of ROI misplacement at different noise levels.

Main results.—In absence of noise and blurring, systematic uncertainties were up to 28.8% and 31.0% with 2D and 3D ROIs, respectively, for the 10-mm sphere, with the highest impact from ROI misplacement. In all cases, smaller spheres showed higher uncertainties with larger voxels. Contrary to prior assumptions, the use of 3D ROIs did not exhibit less susceptibility for parameter changes. Experimental and computer-generated images both demonstrated considerable variations on individual CRC measurements when background coefficient-of-variation exceeded 20%, despite negligible effects on mean CRC.

Significance.—This study underscores the effect of scanner-independent parameters on reliability, reproducibility, and comparability of CRC measurements. Our findings highlight the trade-off between the benefits of smaller voxel sizes and noise-induced CRC fluctuations, which is not considered in the current version of the NEMA IQ standards. The results furthermore warrant adjustments to the standard to accommodate the advances in sensitivity and spatial resolution of current-generation PET scanners.

rbayerlein@ucdavis.edu .

Keywords

positron emission tomography (PET); contrast recovery coefficient; NEMA NU 2; performance evaluation; image quality assessment

1. Introduction

The National Electrical Manufacturers Association (NEMA) NU 2 standardized measurements [1] are commonly used for evaluating the performance of clinical positron emission tomography (PET) scanners. PET image quality (IQ) is typically assessed in a standardized imaging situation aiming to simulate clinical imaging conditions with hot lesions, using the NEMA IQ phantom. As a figure of merit, PET IQ is hereby characterized through measurements of contrast recovery coefficient (CRC) and background variability for spheres of different diameters. CRC measurements aim to quantify the scanner's ability to correctly recover the activity concentration of a hot spherical lesion in a warm background in a reconstructed PET image. The NEMA IQ phantom consists of a radioactive background compartment with a volume of about 9.8 liters filled with ^{18}F in aqueous solution with an activity concentration of 5.3 kBq/mL, a low-density non-radioactive lung insert at the center, and six hot spheres that are arranged circumferentially around the lung insert. The spheres have internal diameters of 10, 13, 17, 22, 28, and 37 mm and are filled with an activity concentration ratio of 4:1 with respect to background according to the NEMA NU 2–2018[1]. In earlier standards, the largest two spheres were filled with non-radioactive water[2].

For a lesion with a given size and activity concentration, CRC is significantly affected by the reconstruction algorithm, and the reconstruction protocol, as well as the scanner characteristics, such as spatial resolution and time-of-flight (TOF) resolution. Furthermore, noise properties of the image affect the reproducibility of the CRC. Particularly, in iterative image reconstruction algorithms, such as the commonly used ordered subsets expectation maximization (OSEM) algorithm, a trade-off between contrast and noise occurs because at higher iterations the algorithm converges to higher-contrast images[3], at the expense of increased correlated noise, as demonstrated previously in experimental data [4, 5]. Similarly, TOF has an indirect impact on CRC by increasing the OSEM convergence rate, resulting in improved contrast recovery and signal-to-noise ratio compared to non-TOF reconstruction with the same number of iterations [6]. The effect of scanner spatial resolution and TOF on lesion contrast has been previously studied in human subjects, where improved spatial resolution and TOF have led to a higher measured lesion contrast and improved quantification using the same number of iterations, as expected [7]. Additional effects on CRC can be expected when resolution modelling (RM), also referred to as point spread function (PSF) modeling, is incorporated into the image reconstruction algorithm, with the aim of modelling the phenomena that degrade the resolution within the system matrix of the reconstruction algorithm. These could include positron range, photon noncollinearity, and detector-related effects. RM generally results in faster convergence and significant improvements in image resolution and contrast [8, 9], which, consequently, leads to higher CRC values for all sphere sizes of the NEMA IQ phantom, as demonstrated for

example by Spencer et al. 2020[4]. It might be worth noting that the use of RM proves most impactful for contrast and lesion detectability when TOF-based reconstruction is used[10]. However, RM can cause artifacts near sharp boundaries, similar to the commonly known Gibbs phenomena in truncated Fourier series, which can distort CRC measurements by causing ringing artifacts or unexpectedly higher results for individual sphere sizes [8]. This has been demonstrated in image quality assessments of the Biograph Vision Quadra (Siemens Healthineers, Knoxville, TN, USA) [5] and Biograph Vision (Siemens Healthineers, Knoxville, TN, USA) [11] PET/computed tomography (CT) systems.

In addition to scanner- and reconstruction-dependent factors, CRC measurement is also affected by some scanner-independent systematic uncertainties, introduced by partial volume effects due to image voxelization. In clinical PET imaging partial volume effects can be observed as contributions from different tissue types with potentially different tracer uptake that are combined in a single voxel (tissue-fraction effect) [12]. In scans of the NEMA IQ phantom partial volume can cause degradation of the contrast. The magnitude of these effects is governed by parameters such as voxel size, sphere position relative to the image grid, placement of the region of interest (ROI), or a combination of all the above. In general, using smaller voxel sizes is expected to improve the CRC, due to reduced partial volume effect. This has been shown in several studies, including Epley et al. (2018) who quantitatively demonstrated the benefit of using smaller voxel sizes for contrast recovery of an 8-mm lesion with a 2.5:1 lesion-to-background activity concentration ratio [13]. Similarly, Koopman *et al.* (2017) reported that phantoms with spheres of 13 mm or less show higher CRC values with 2-mm isotropic voxel sizes compared to 4 mm[14]. The position of the spheres on the underlying grid in the reconstructed image is almost impossible to control in a realistic scan and therefore poses another source of uncertainty on the CRC. Mansor *et al.* (2017) used 12 scans of the NEMA IQ phantom to demonstrate that randomly repositioning the phantom (over a range of less than 2 cm) has an impact on quantitative PET[15]. They also found that the impact of the phantom position on the contrast was furthermore dependent on the voxel size, and that larger voxel sizes would show larger susceptibility to position changes. Finally, a misplacement of the ROI will cause a reduction of the calculated activity concentration enclosed by that ROI and will therefore have a direct impact on the CRC. The magnitude of this effect and its relation to other parameters have not been quantified to date and are therefore subject of this study.

The NEMA NU2 CRC measurements performed on state-of-the-art commercial PET scanners [4, 5, 11, 16, 17, 18, 19] show a general trend towards an increased CRC with increasing sphere size and decreasing voxel size. However, there are prominent deviations in the experimental results, examples of which are shown in Figure 1 in a comparison of the NEMA NU 2–2018 CRC measurements performed on four different PET/CT scanners, all using different implementations of the TOF-OSEM image reconstruction algorithm with RM. This includes the Vereos Digital PET/CT (Philips Healthcare, Amsterdam, The Netherlands) using 2-mm isotropic voxels, 3 iterations, and 17 subsets, the Biograph Vision (Siemens Healthineers, Knoxville, MA, USA) using 1.6-mm isotropic voxels, 8 iterations, and 5 subsets, the Biograph Vision Quadra (Siemens Healthineers, Knoxville, MA, USA) using 1.65-mm isotropic voxels, 8 iterations, and 5 subsets, and the uEXPLORER total-body PET/CT scanner (United Imaging Healthcare, Shanghai, China) using 1.17-mm isotropic

voxels, 4 iterations, and 20 subsets. While the NEMA protocol aims to compare the image quality of different scanners for clinically used settings, the different image reconstruction implementations, and different voxel sizes in combination with the different levels of convergence, in addition to physical and geometrical differences of the scanners, make the comparison of the results between individual scanners challenging. Nevertheless, when evaluating CRC measurements of individual scanners, certain anomalies can be observed, where CRC is not increasing monotonically as the sphere size is increased. This can be seen in the CRC results of the uEXPLORER, where the highest CRC is obtained with the 17-mm sphere, and also for both the Vision and the Vereos, where the 22-mm sphere yields larger CRC compared to the 28-mm sphere. Finally, both the Biograph Vision and the Biograph Vision Quadra show unexpectedly higher CRCs for the smallest sphere. While this might be a result of the Gibbs-like phenomenon, which particularly affects small objects [11, 16], and has been assumed by the conductors of these measurements, it could also originate from voxelization effects, or a combination of both effects.

These observed anomalies have fueled the interest in a thorough investigation of scanner-independent systematic uncertainties in the CRC measurements of the NEMA IQ phantom. Although the general trends and the sources of these uncertainties are well-understood, the magnitude of the introduced errors into CRC measurements have not been quantified to date. In this work, the errors introduced by scanner-independent systematic uncertainties are quantified numerically using computer-generated images of a NEMA IQ-like phantom. This approach provides the benefit of taking scanner-dependent effects and the reconstruction process out of the equation and allows for an investigation of the partial volume effect due to image voxelization on the outcome of CRC measurements in PET with purely numerical methods.

In this work, the systematic uncertainties on the calculated CRC values have been calculated for all six spheres of the NEMA IQ phantom, originating from variations in voxel size, sphere placement, and ROI alignment. Image noise or smoothing is expected to reduce the impact of these parameter changes on the obtained CRC values; however, the extent of this mitigation is not well understood. This is particularly interesting for the state-of-the-art PET scanners, which offer improved spatial resolution and sensitivity, in which the voxelization effects on CRC curves may become more prominent in absence of post-reconstruction smoothing. To investigate these assumptions and to quantify the fluctuations of CRC in the presence of noise, Poisson noise was added to computer-generated images, and a Gaussian filter was used to mimic detector blurring.

Lastly, we present a comparison of our findings to CRC measurements performed on experimental image data, subsampled to different noise levels, obtained from NEMA IQ scans performed on the uEXPLORER PET/CT scanner – a total-body imaging camera with a 194-cm-long axial field of view [20]. The scanner provides an up to 68-fold increase in sensitivity compared to conventional PET scanners for whole-body imaging and has a NEMA spatial resolution of 3.0 mm FWHM [4].

This work has implications for the reliability, comparability, and reproducibility of image quality assessments obtained via the CRC analysis of the NEMA IQ phantom for all

previous and future scanner characterizations [1, 2, 21]. Use of 3-dimensional (3D) ROIs – often referred to as volumes of interest (VOIs) – instead of 2-dimensional (2D) ROIs has been proposed and was investigated for the CRC calculation regarding its ability to mitigate above effects. Early NEMA standards used 2D ROIs most likely for computational reasons, which in modern times are much less an issue for image analysis.

2. Materials and methods

2.1. Computer-generated noise-free images

3D voxelized images of the NEMA NU2 IQ phantom were generated in MATLAB R2020b v9.9.0 (MathWorks, Natick, MA, USA), containing six hot spheres with diameters of 10, 13, 17, 22, 28, and 37 mm embedded in a warm background. The activity distribution was a noise-free representative of an ideal image, to exclude the effects from scanner sensitivity, spatial resolution, and image reconstruction software, and exclusively quantify the theoretical uncertainties in CRC measurement, due to image voxelization, sphere position with respect to the image grid, and the ROI analysis method. Spheres of given radii were discretized on the underlying image grid. A voxel was given a value of 4.0, representing the activity concentration in the spheres, if its distance from the sphere's center was smaller than the sphere's radius and was otherwise given a value of 1.0. The center of each sphere was initially assigned to the center of a voxel. To take into account partial volume effects at the spheres' edges due to voxelization, each voxel was sub-divided into 125,000 sub-voxels (i.e., 50×50×50). The value of these voxels was then determined by the fraction of sub-voxels that lie within a distance to the sphere's center smaller or equal to the radius of the sphere, as shown in an example image generated using 2.85-mm isotropic voxels in Figure 2. A sphere-to-background activity concentration ratio of 4:1 was used for all images, although it must be noted that the numerical analysis in this section will be independent of the activity concentration ratio.

2.2. Calculation of contrast recovery coefficient

An image quality assessment based on the NEMA NU 2–2018 protocol was performed to measure the CRC of each sphere. 2D ROIs were placed on the image slice where the centers of the spheres were located using a semi-automated process, and the average activity concentration was calculated for each ROI. For computer-generated images the centers of the ROIs were aligned with the sphere's center, while in experimental images, the ROIs were scanned over the spheres in a range of ±2 voxels in x- and y-direction in steps of 0.01 voxels and the location with the highest average activity concentration was taken. Additionally, in accordance with the NEMA standard, twelve ROIs were placed in the warm background on five consecutive central image slices (i.e., 60 ROIs in total) to calculate the mean background activity concentration. The mean activity concentration in each ROI was calculated from the weighted average of all voxels within the ROI, in which a weighting factor in the range of 0 to 1 was used for each voxel corresponding to the fraction of sub-voxels contained within the ROI. Each voxel was divided into 8000 sub-voxels (20×20×20) for the calculation of the weighting factor.

2.3. Investigated parameters

To study the effect of voxel size on CRC uncertainty, noise-free images of the NEMA IQ phantom were generated using isotropic voxel sizes of 1.6 mm, 2.85 mm, and 4.0 mm, thereby covering a reasonable range of typical voxel values. The 2.85-mm voxels correspond to the standard voxel size of the UC Davis in-house reconstruction framework, while the vendor's reconstruction software uses 2.344 mm voxels for clinical studies (see section 2.7. Experimental PET image data). Furthermore, CRC uncertainty varies by the total share of voxels that are affected by partial volume effects due to voxelization and is consequently affected by the sphere size. Therefore, a second set of noise-free images was generated for sphere diameters in the range of 5 mm to 40 mm, in steps of 1 mm, with each sphere being modeled separately on a warm background.

To study the effects from ROI misplacement and sphere position relative to the image grid on CRC calculation, noise-free images of the six sphere sizes of the NEMA NU 2 IQ phantom were generated with an isotropic voxel size of 2.85 mm, corresponding to the default voxel size of the UC Davis in-house PET image reconstruction framework [22]. The ROIs were first shifted with respect to the spheres' centers in an interval between 0 and 1 voxels in steps of 0.1 voxels. Second, each sphere was shifted by up to 0.5 voxels in one dimension in steps of 0.1 voxels, keeping the ROIs aligned and centered on the spheres. CRC was calculated in each case for the six investigated sphere sizes. Table 1 summarizes all investigated parameters.

2.4. Estimation of systematic uncertainties

The above listed scanner independent parameters pose a source for systematic uncertainties on the calculated CRC for each sphere. The upper bound on the uncertainties was estimated in the investigated parameter space for each sphere of the NEMA IQ NU 2 phantom separately, by calculating the square-root of the summed squares of the largest CRC deviation from the default value introduced by the individual parameters:

$$\sigma = \sqrt{\sigma_{vox}^2 + \sigma_{ROI}^2 + \sigma_{sp}^2} \quad (1)$$

where σ_{vox}, σ_{ROI} and σ_{sp} are defined as the maximum CRC deviations from the default value due to variations in voxel size, ROI placement, and sphere position, respectively. The default CRC value was calculated using the parameters listed in the third column of Table 1.

2.5. Using 3D ROIs

NEMA standard suggests use of 2D ROIs placed onto the central image slice of the spheres for the CRC measurement[1]. This method is susceptible to errors in phantom positioning, resulting in selection of a nonoptimized slice for all spheres. It is, however, unclear whether using 2D ROIs suffers from larger uncertainties in CRC measurement compared to using 3D spherical ROIs. The fraction of voxels that lie at the edge of the ROI and that are only partially covered by the ROI contribute to partial volume effects. This fraction is different for 2D ROIs and 3D ROIs, which suggests the need for also exploring the use of 3D

ROIs and investigating their susceptibility to scanner independent parameters. To quantify the uncertainties in CRC measurement in absence of the effects from statistical noise, the influence of voxel size, ROI misalignment, and sphere placement was examined for 3D ROIs and was compared to the CRC calculated following NEMA standard with 2D ROIs. Also, the systematic uncertainties were calculated using 3D ROIs and compared to the results from the NEMA standard.

2.6. Including Poisson noise and Gaussian blurring

Next, since PET reconstructed images include blurring effects due to finite spatial resolution of the detectors, a Gaussian smoothing kernel with a full-width-at-half-maximum (FWHM) of 3.0 mm was applied to the noise-free images. This value represents the spatial resolution of the uEXPLORER total-body PET scanner [4]. To model the effect of statistical noise present in PET reconstructed images, a simplified model was used where Poisson noise was artificially added to computer-generated Gaussian-smoothed images. It should be mentioned that this is an approximation as the image noise in iteratively reconstructed PET images is not strictly Poisson but correlated.

Then, the effects of voxel size, ROI misalignment, and sphere position on the image grid were investigated with the noisy images. The computer-generated noise-free image was first scaled; Poisson noise was subsequently added to the image by interpreting each voxel value as the mean of a Poisson distribution and the image was rescaled with a division by the scaling factor. As a measure of the image noise level, the coefficient of variation (CV) was measured in the 60 2D ROIs with 37 mm diameter placed on the warm background, defined as:

$$CV = \frac{\sigma}{\mu}, \tag{2}$$

where σ is the standard deviation of all voxels in all background ROIs and μ represents their mean value. Images with CVs between 10.0% and 44.6% were generated, corresponding to scaling factors ranging from 5 to 100. Table 2 lists all computer-generated images with their corresponding scaling factors and CVs. Figure 3 shows four examples of computer-generated images including Poisson noise, with CV varying from 10.0% to 44.6%. A voxel size of 2.344 mm was chosen, matching the uEXPLORER vendor-reconstructed images, allowing for a better comparison between the computer-generated images and the experimental images. For every noise level, 30 realizations were created, and the mean and standard deviation of the CRC was calculated. Subsequently, the effects of sphere placement and ROI misalignment on CRC were re-evaluated in presence of noise and detector blurring. Finally, the impact of voxel size on the CRCs measured in blurred noisy images was investigated, in 30 noisy realizations of the NEMA IQ-like image with CV of 19.7%, using isotropic voxel sizes of 1.6 mm, 2.344 mm and 4.0 mm.

2.7. Experimental PET image data

The findings from the numerical simulations were compared to the CRCs measured on experimental PET images obtained with the uEXPLORER total-body PET scanner. A NEMA NU 2 IQ phantom with a sphere-to-background activity concentration ratio of 3.9 to 1 was scanned for 30 min following the NEMA NU 2–2018 protocol. The list-mode dataset was randomly subsampled to create multiple fully independent noisy datasets, each with a predefined fraction of the total amount of the original list-mode events representing virtual frame lengths with identical count density. Using subsampling ratios (SR) of 1/180, 1/90, 1/60, and 1/30, virtual frame lengths of 10 s, 20 s, 30 s, and 60 s were created, with 30 realizations each. Furthermore, 15 realizations with a subsampling ratio of 1/15, 10 realizations with a subsampling ratio of 1/10, and 6 realizations with a subsampling ratio of 1/6 were created, representing virtual frame lengths of 120 s, 180 s, and 300 s, respectively. Images were reconstructed with the vendor's image reconstruction software, using a list-mode TOF-OSEM algorithm with 4 iterations, 20 subsets, and a 2.344-mm isotropic voxel size. No PSF modeling was used, and no post-reconstruction filter was applied. These reconstruction parameters were selected based on the standard clinical reconstruction protocol at our institution [23]. Similar to the previous section, the noise level was quantified using CV, with values ranging from 11.8% to 63.0%. Mean and standard deviation of the CRCs were calculated from all realizations of each subsampling ratio.

Figure 4 shows the reconstructed images of four examples of the subsampled datasets generated from a 30-min scan of the NEMA NU2 IQ phantom on the uEXPLORER, with CVs varying from 11.8% to 44.5%. Table 3 provides a full overview of all generated datasets together with their corresponding subsampling ratios, CV, and the number of realizations. The reconstructed images of the subsampled datasets were subsequently analyzed to quantify the CRC variations due to ROI misalignment, by shifting the ROIs by 0.5, 0.8 and 1.0 voxels for all available noise levels and measuring the CRC at each step.

3. Results

3.1. Computer-generated noise-free, unblurred images

Voxelization effect on the CRC for different sphere sizes—Figure 5 (a) shows the calculated CRC for sphere sizes in the range of 5 mm to 40 mm, using three different voxel sizes of 1.6 mm, 2.85 mm, and 4.0 mm. The CRC curves show fluctuations which grow larger as the sphere size is decreased and voxel size is increased, in which the oscillation periods seem to be correlated with the voxel sizes. Higher CRCs are observed on average when smaller voxel sizes are used, as expected. However, due to the large fluctuations of the CRC, exceptions can be observed in some datapoints, in which CRCs of a given sphere size are higher when a larger voxel size is used (e.g., using a voxel size of 4.0 mm yields a higher CRC than using 2.85-mm voxels for sphere sizes of 5 mm, 6 mm, 12 mm, 13 mm, and 29 mm). Similar CRC fluctuations were also observed when CRC measurements were plotted for any given sphere size of the NEMA IQ phantom as a function of voxel size, as shown in supplementary figure 1, in which the magnitude of CRC fluctuations was substantially higher in smaller spheres with larger voxels. Similarly due to the large fluctuations in CRC, it can be observed that CRC is not always higher for larger sphere sizes at a given voxel size.

Figure 5 (b) shows the CRC as a function of the sphere size, calculated using spherical 3D ROIs. A general trend can be observed when comparing the 2D and the 3D analysis results, in which the CRC values obtained with 3D ROIs are lower than with 2D ROIs. For the 1.6 mm, 2.85 mm, and 4.0 mm voxels, the 3D ROIs yield 2.9 %, 4.7%, and 5.2% lower values, respectively, on average over the displayed sphere size range. However, in contrast to 2D ROIs, using 3D ROIs reduces the amplitude of the oscillations of the CRC for some sphere sizes in the NEMA-relevant range starting at 10 mm. Considering the example of 4.0-mm voxel size, the difference between the CRC of the 17 mm and 21 mm sphere is 10.7% using 2D ROIs and 8.0% using 3D ROIs, respectively.

Effect of ROI misplacement—Figure 6 shows the effect of ROI placement error of up to one voxel on the calculated CRC of the six spheres of the NEMA NU 2 IQ phantom, when 2D ROIs ((a), (c), and (e)) or spherical 3D ROIs ((b), (d) and (f)) are used with isotropic voxel sizes of 1.6 mm, 2.85 mm, and 4.0 mm. As expected, sub-voxel misplacement of the ROI leads to underestimation of CRC in all cases; and larger underestimations are observed as the ratio of the misplacement error to sphere size increases (i.e., larger effects with larger voxel sizes and smaller sphere sizes). Shifting a 2D ROI up to one voxel could lead to 3.3% – 8.7% underestimation of the CRC for the 37-mm sphere using voxel sizes of 1.6 – 4.0 mm, respectively, whereas CRC underestimation up to 10.3% –22.5% is observed for the 10-mm sphere. In all cases, the percentage changes represent the absolute changes in CRC, which itself is expressed in percentage. While using 3D ROIs leads to lower CRC values in all cases, as expected, the percentage of CRC underestimations due to ROI misplacement are similar to using 2D ROIs, ranging from 3.3%– 8.4% in case of the 37 mm sphere to 11.2% – 21.1% with the 10-mm sphere.

Effect of the sphere position on the image grid—Figure 7 shows the CRC values obtained with 2D ROIs and spherical 3D ROIs, when the sphere position on the image grid is shifted up to half a voxel, using three isotropic voxel sizes of 1.6 mm, 2.85 mm, and 4.0 mm. Due to the symmetry and absence of noise, there is a periodicity in changes of CRC, such that shifting the sphere center position by 0.1 voxels yields the same CRC as a shift by 0.9 voxels. Similar to the ROI placement errors, larger effects on the calculated CRCs can be observed when the ratio of the voxel size to sphere diameter is increased; however, overall, the magnitude of the effects resulting from sphere positioning on the image grid is smaller than for ROI misplacements, and a sphere position shift from the voxel center does not necessarily translate into reduced CRC. As expected, the largest effect is observed with the 10 mm sphere, in which the 2D ROI CRC increases by 5.1% when the sphere position is shifted off-center by 0.5 voxels, using a 4.0-mm isotropic voxel size, and the CRC changes up to 2.3% in the case of 1.6-mm voxel size. The effect is evidently reduced for larger sphere sizes, where in the case of the 37-mm sphere, CRC changes of 0.3% and 1.5% were observed with the 1.6-mm and the 4.0-mm voxels, respectively.

Furthermore, a shift of the sphere can result in non-monotonic increase of the CRC as a function of sphere size, as commonly observed in some experimental results [5, 11]. As an example, with 2.85-mm isotropic voxels, positioning the spheres at the center of an image voxel (i.e., no shift) results in lower CRC for the 13-mm sphere compared to the 10-mm

sphere; whereas, when the spheres are shifted, the curve becomes monotonic. A similar effect can be observed for the 13-mm and the 17-mm spheres when 4.0-mm isotropic voxel size is used.

Using 3D spherical ROIs mitigates the effects of sphere position on the calculated CRC. The effect of the sphere position shift on the calculated CRC of the 10-mm sphere is reduced from 2.3% to 1.0% in the case of the 1.6-mm voxels, and from 5.1% to 4.1% for the 4.0-mm voxels. Sphere sizes above 22 mm show almost no deviation resulting from a sphere shift.

Systematic uncertainties of the CRC measurement in the absence of noise— The combined effect of the studied parameters results in systematic uncertainties of the calculation of the CRC, which are shown in Figure 8 for the NEMA IQ sphere sizes using 2D and 3D ROIs. The systematic uncertainties increase with decreased sphere size, as expected, and for 2D ROIs range from 6.5% for the largest sphere to 28.8% for the smallest sphere of the NEMA IQ phantom, and for 3D ROIs range from 6.7% to 31.0%.

3.2. Computer-generated images with Poisson noise and Gaussian blurring

Effect of noise—Figure 9(a) shows the mean CRC measured on 30 blurred and noisy realizations of the NEMA IQ image, generated with three different noise levels with corresponding CVs varying from 10.0% to 44.7%. The results are compared to an ideal noise-free, unblurred images. The standard deviation of the measured CRC values on the 30 noisy realizations of the NEMA IQ image are additionally shown in Figure 9(b). All three mean CRC curves from noisy images yield similar values independent of their noise level, and any deviations are well within the standard deviation; however, the standard deviation strongly depends on the noise level and increases with increased noise and smaller sphere sizes, as expected. The ideal noise-free and unblurred image of the same voxel size shows up to 12.7% and 2.3% larger CRC for the sphere sizes of 10 mm and 37 mm, respectively.

Effect of Voxel size in the presence of noise—Figure 10 shows the CRC measured on 30 noisy realizations of the NEMA IQ image quantified with a CV of 19.7%, generated with three different isotropic voxel sizes of 1.6 mm, 2.344 mm, and 4.0 mm. The error bars indicate the standard deviation of the CRC measurements. While all CRC measurements for all three voxel sizes show decreased CRC compared to the noise-free and unblurred case, certain features caused by voxelization are preserved as shown by the dip at 17-mm sphere size in case of 4.0-mm voxels, which was also observed in the noise-free case (see figure 7(e)). Moreover, larger sphere diameters seem negligibly affected by a change of voxel size, and they show similar measured CRCs.

Effect of ROI misplacement in the presence of noise—Figure 11 (a) shows the effect of ROI misplacement on the mean CRC values measured on 30 noisy realizations of the NEMA IQ image generated with a CV of 19.7%. An ROI shift by one voxel in the noisy image causes a CRC underestimation between 9.5% and 3.4% for the 10-mm and 37-mm sphere sizes, respectively, which are slightly lower than the 13.7% and 4.4% underestimations obtained by one-voxel shift on the noise-free, unblurred image. Additionally, Figure 11 (b) shows the effect of an ROI misplacement by one voxel of the

NEMA IQ image generated with 3 different noise levels, with corresponding CV values between 10.0% and 44.7%. Independent of the noise level, the mean CRC is on average reduced by the same value in all three cases and the deviations are well within the calculated standard deviations.

Effect of the sphere position on the image grid in presence of blurring and noise—Figure 12(a) shows the effect of changing the sphere position on the image grid on the mean CRC values measured on 30 noisy realizations of the NEMA IQ image generated with a CV of 19.7%. Shifting the spheres on the underlying image grid by half a voxel causes CRC drifts of 3.2% and 0.1% compared to the default central sphere positions for the 10-mm and 37-mm sphere sizes, respectively, whereas in the noise-free, unblurred image, the same sphere shift causes deviation of 4.7% and 0.1%, respectively. Figure 12(b) compares the effect of half a voxel sphere shifting on the mean CRC values measured on 30 noisy realizations of the NEMA IQ image generated with 3 different noise levels, with corresponding CV values between 10.0% and 44.7%. Similar to the previous section, negligible effects from noise level are observed on the mean CRC values while the position deviations lie within the calculated standard deviations.

3.3. Experimental PET image data

Effect of noise—Figure 13(a) shows the mean CRC measured on multiple realizations of the uEXPLORER images of the NEMA IQ phantom subsampled at various noise levels with corresponding CV values of 11.8%, 25.6% and 44.5%, representing subsample ratios (SR) of 1/6, 1/30, and 1/90 from a NEMA standard 30-minute acquisition duration, respectively. Any deviations observed among the individual mean CRC values are within the corresponding standard deviations shown in Figure 13(b). The standard deviation expectedly increases at higher noise levels, similar to the computer-generated images with noise, however, the standard deviation of the CRC is larger in experimental images than in computer-generated images with added Poisson noise and Gaussian blurring. Since the sphere position on the image gird is close to impossible to control in an experiment, these errors are inherently included in the results.

Effect of ROI misplacement—Figure 14(a) shows the effect of ROI misplacement of up to one voxel on mean CRC values measured on multiple realizations of the uEXPLORER images of the NEMA IQ phantom, subsampled by a factor of 1/30, corresponding to a noise level with a CV of 25.6%. Like computer-generated images, the uEXPLORER images show a clear susceptibility to ROI misalignment, however, slightly less prominently: the absolute CRC underestimations were 8.4% and 2.3% for the 10-mm and 37-mm spheres, respectively, whereas for the computer-generated noisy images the CRC decreased by 9.5% and 3.4%, respectively. Figure 14(b) additionally shows the effect of one-voxel ROI misplacement on the mean CRC values measured on multiple realizations of the uEXPLORER images of the NEMA IQ phantom, subsampled at different noise levels with corresponding CVs between 11.8% and 44.5%. Like in computer-generated images, the mean CRC changes due to ROI misplacement are independent of the noise level. All three depicted noise levels show similar mean CRC vales and deviations are within the calculated standard deviations.

4. Discussion

4.1. Systematic uncertainties due to scanner independent parameters

The three investigated parameters of voxel size, ROI misplacement, and sphere position on the image grid pose a source of systematic uncertainties in the NEMA IQ CRC measurements. These uncertainties have been shown to depend on the sphere size, as expected, varying from 6.5% in case of the 37-mm sphere up to 28.8% with the 10-mm sphere, in absence of detector response blurring and statistical noise, when 2D ROIs are used. The current generation of PET scanners are expected to have similar uncertainties when comparing the CRC of the larger spheres of the NEMA IQ phantom. However, particular attention must be given to measurements of the smaller spheres with regards to reproducibility, reliability, and comparability of quantitative image quality assessment given their higher susceptibility to systematic variations.

In case of noise-free, unblurred computer-generated images, the effect of voxel size on CRC measurements was quantified and was shown to be more pronounced for larger voxels. The general trend towards lower CRC values observed with larger voxel sizes is expected due to an increased partial volume effect, however, the higher fraction of partial voxels contributing to the ROI results in larger fluctuations in the CRC measurement for smaller ROI sizes. In images with added Poisson noise and simulated detector blurring, the effect of voxel size on the CRC measurement is significantly reduced especially for larger sphere diameters, where all three investigated voxel sizes yielded little variations in the obtained CRC, as shown in Figure 10. While using the same voxel size might improve comparability of CRC results obtained in different acquisitions or on different scanners, scanner dependent influences, reconstruction algorithm, and image noise will remain as limiting factors.

Sub-voxel ROI misplacement was shown to have the largest effect on the CRC measurements with up to 22.5% CRC underestimation observed in case of the 10-mm sphere using 4.0-mm voxels. Smaller sphere sizes are more affected, and the magnitude of this effect increases for larger voxel sizes, as expected (Figure 6). On the other hand, an ROI misplacement reduces the number of partial voxels contributing to an ROI, which was found to smooth out the non-monotonic behavior of the CRC-curves. These findings point out the necessity of utilizing standardized analysis tools, which most importantly comprise a well-designed, semi-automated procedure for accurate placement of the ROIs.

Furthermore, the exact position of the sphere on the underlying image grid has been shown to have smaller effects on the CRC measurements than ROI misplacement and voxel size (Figure 7). However, CRC errors of up to 5% were observed with the 10-mm sphere using 4.0-mm voxels. As expected, images with larger voxels were more affected.

Effects of ROI misplacement and sphere position on CRC measurements were still considerable, when Poisson noise and Gaussian blurring were included in the computer-generated images, and CRC was up to 9.5% underestimated. Additionally, the effect of ROI misplacement on CRC measurements could also be confirmed with the experimental image data, in which up to 8.4% CRC underestimation was observed. The peculiar bump in the CRC at 17-mm sphere size in the experimental image data (Figure 14(a)) could originate

from voxelization effects and the specific sphere position on the image grid, as a similar feature has been observed in computer-generated image data independent of their noise level as seen in Figure 12(b).

Introducing the Gaussian blurring into images reduced the effects from ROI misplacement and sphere position. The effect of an ROI misalignment of one voxel was reduced by up to 4% in images with Gaussian blurring and Poisson noise compared to the noise-free unblurred images. Despite the existence of semi-automated positioning tools using high-quality CT scans, investigations of ROI misplacements are necessary since we could show that even with a small voxel size of 1.6 mm a sub-voxel ROI misplacement can cause up to 3% difference in CRC.

Similarly, sphere position changes of 0.5 voxels had about 1% less influence in noisy and blurred images compare to noise-free, unblurred ones. Despite the relatively small effect of sphere positioning observed in this study, in experimental scans of the NEMA IQ phantom, it is almost impossible to predict or to control the position of the sphere centers with respect to the grid of the reconstructed image. And according to the NEMA protocol, images should be reconstructed using the standard parameters for whole body studies [1] limiting the options for adjustments of the image grid after data taking. Therefore, the sphere position will remain a factor of systematic uncertainty to be considered.

4.2. Exploring the use of 3D ROIs

The use of 3D ROIs instead of 2D ROIs for CRC measurements has proven to somewhat mitigate the effects from voxelization and sphere position on the image grid, however, contrary to prior expectations, using 3D ROIs did not yield lower systematic uncertainties, as shown in Figure 8. 3D ROIs provide an average over more partial voxels than 2D ROIs, therefore showing smaller fluctuations in the CRC curve for sphere diameters in the range from 5 mm to 40 mm for the three investigated voxel sizes of 1.6 mm, 2.85 mm and 4.0 mm (Figure 5). Nevertheless, the CRC values for the six NEMA IQ sphere diameters happen to be similarly affected by voxel size for both 2D and 3D ROIs, therefore, contributing to the systematic uncertainty to similar extent within the given parameter space.

Furthermore, CRC measurements using 2D and 3D ROIs are similarly affected by ROI misalignments, and no improvement of the reliability of CRC measurements can be expected by using 3D ROIs instead of 2D ROIs. The effect of sphere position on the image grid was only marginally reduced by the use of 3D ROIs compared to 2D ROIs, and since this effect was small to begin with, the improvement with 3D ROIs did not have an appreciable influence on the total systematic uncertainty, nor improve the reproducibility of CRC measurements. Furthermore, lower CRC values are obtained with 3D ROIs compared to 2D due to the higher fraction of partial voxels contributing to the 3D ROI. Considering the marginal benefit in reduction of systematic uncertainty from using 3D ROIs our findings do *not* warrant a suggested change to the NEMA standard analysis. Nevertheless, 3D ROIs might still be a better choice, because now all scanners use 3D reconstructions and therefore 3D ROIs can better capture the 3D reconstruction artifacts such as the Gibbs artifact.

One limitation of this investigation was that only one-dimensional shifts of the sphere position on the underlying image grid and the ROI position on the spheres were evaluated. The quantitative results might change if other dimensions were included.

4.3. The effect of image blurring and noise

Negligible effects from increased Poisson noise on the mean CRC measurements can be observed, in both computer-generated (Figure 9(a)) and experimental images (Figure 13(a)). Thus, the reduction of mean CRC in noisy, blurred images compared to the CRC in noise-free, unblurred images originates from the blurring introduced by the Gaussian filter rather than the Poisson noise.

Despite the largely unaffected mean CRC, considerable variations occurred between the results of individual CRC measurements, constituting a limiting factor for the reproducibility of CRC measurements. In the case of conventional PET scanners with limited sensitivity, individual scans of the NEMA IQ phantom could result in CRC measurements with substantial deviations from one another, especially for the smaller sphere diameters. Additionally, noise in the background has the potential to create a global bias to the CRC of all spheres, which is especially impactful for conventional scanners. Although background variability is included as a part of the NEMA IQ analysis as a figure of merit that intrinsically includes effects from statistical noise, as well as nonuniformities that could be a result of errors in the normalization, we believe that additional reports on the CV as a direct measure of noise could be beneficial for comparability of the results. Furthermore, the 30-min standard acquisition of the NEMA IQ phantom might not be sufficient to compare CRC measurements of different scanners in the same source count setting, due to differences in scanner sensitivities. Performing a significantly longer scan of the phantom, beyond 30 min, would be beneficial for obtaining reference CRC values that are more representative of the mean CRC measurements. This would provide the opportunity to perform additional reconstructions with smaller voxel sizes than at clinical conditions, while limiting the influence of noise and could provide more informative results, particularly in cases where large fluctuations in the CRC curves are expected due to voxelization. Since performing multiple fillings and scans of the NEMA IQ phantom is technically impractical, multiple delayed scans of the phantom or shorter frames of the original scan should be analyzed and compared to the reference CRC measurement to quantify the noise effects on the CRC measurement in different scenarios.

Lastly, the CRC analysis performed on the experimental image data are in good agreement with the computer-generated images that include noise and blurring, with a similar magnitude of the mean CRC changes observed due to ROI misplacement and the introduction of noise. The experimentally measured mean CRC for all spheres is lower than the CRC on computer-generated images – which is independent of the noise level. This difference is due to scanner specific properties and depends on the reconstruction algorithm and its parameters. Besides that, the standard deviation of the CRC measurements in the experimental image data is larger than the computer-generated images, when compared at similar noise levels quantified by background CV. This may be attributed to the convergence of the reconstruction algorithm and the fact that the noise in iteratively reconstructed PET

images is not strictly Poisson but correlated and often rotation symmetric or isotropic [24] and are apparent in Figure 4. Especially when resolution modeling (RM) is included, the noise distribution in the image can get substantially altered [16]. Based on the previously mentioned references [5, 8] to the potential occurrence of Gibbs-like artifacts, one could make the recommendation of performing NEMA IQ CRC measurements both with and without RM.

As an alternative to using numerically generated images with added Poisson noise, reconstructed images from simulation data could be used, which would show similar correlated noise patterns as the real images. Numerical images provide the advantage of singling out every individual voxelization effect in the absence of noise which is crucial for an understanding of the impact of each of the scanner-independent parameters on the measured CRC and for the calculation of the systematic uncertainties. However, we would like to mention the advantage of simulations over experimental data in terms of position control of the spheres on the underlying image grid, which is why simulation data taken with SimSET are subject to ongoing investigations.

5. Conclusion

In this work, we have demonstrated and quantified the magnitude of the effects from three scanner-independent parameters on the CRC measurements of the NEMA IQ phantom used in image quality assessment of clinical PET scanners. This includes the effects from changing the voxel size, alignment of the ROI on the individual spheres of the phantom, and the exact position of the spheres on the underlying image grid. These influences pose a source of systematic uncertainties on the measured CRC, which could vary between 6.5% and 28.8% when 2D ROIs are used, in addition to the inevitable uncertainties due to statistical noise. In the presence of blurring and noise, the average CRC obtained from several noisy realizations of the image is slightly less affected by these systematic uncertainties, however, large deviations can occur between individual measurements. Against prior expectations, using 3D ROIs could not substantially mitigate these systematic uncertainties compared to 2D ROIs. Our findings have important implications for the improvement of the next iteration of the NEMA standard for quantitative image quality assessment of PET scanners with one main goal being to limit the impact of noise and voxelization on the CRC measurement. Any changes to the standard must be particularly adapted to the significant advances in sensitivity and spatial resolution of the current-generation PET scanners.

Supplementary Material

Refer to Web version on PubMed Central for supplementary material.

Acknowledgement

This study received funding through NIH grant R01 CA206187 and R01 CA24942 and from a research grant from United Imaging Healthcare.

References

[1]. NEMA standards publication NU 2–2018 – performance measurements of positron emission tomographs (PET), National Electrical Manufacturers Association, 2018

[2]. NEMA standards publication NU 2–2012 – performance measurements of positron emission tomographs (PET), National Electrical Manufacturers Association, 2012

[3]. Lois C, Jakoby B, Long M, Hubner K, Barker D, Casey M, Conti M, Panin V, Kadrmas D and Townsend D, "An assessment of the impact of incorporating time-of-flight information into clinical PET/CT imaging," J Nucl Med, vol. 51, no. 2, pp. 237–45, Feb 2010 [PubMed: 20080882]

[4]. Spencer B, Berg E, Schmall J, Omidvari N, Leung E, Abdelhafez Y, Tang S, Deng Z, Dong Y, Lv Y, Bao J, Liu W, Li H, Jones T, Badawi R and Cherry S, "Performance Evaluation of the uEXPLORER Total-Body PET/CT Scanner Based on NEMA NU 2–2018 with Additional Tests to Characterize PET Scanners with a Long Axial Field of View," J Nucl Med, vol. 62, no. 6, pp. 861–870, 1 June 2021 [PubMed: 33008932]

[5]. Prenosil G, Sari H, Fürstner M, Afshar-Oromieh A, Shi K, Rominger A and Hentschel M, "Performance Characteristics of the Biograph Vision Quadra PET/CT System with a Long Axial Field of View Using the NEMA NU 2–2018 Standard," J Nucl Med, vol. 63, no. 3, 2022.

[6]. Surti S, "Update on time-of-flight PET imaging," J Nucl Med, vol. 56, no. 1, pp. 98–105, Jan 2015 [PubMed: 25525181]

[7]. Surti S, Viswanath V, Daube-Witherspoon M, Conti M, Casey M and Karp J, "Benefit of Improved Performance with State-of-the Art Digital PET/CT for Lesion Detection in Oncology," J Nucl Med, vol. 61, no. 11, pp. 1684–1690, Nov 2020. [PubMed: 32198313]

[8]. Rahmim A, Qi J and Sossi V, "Resolution modeling in PET imaging: theory, practice, benefits, and pitfalls," Med Phys, vol. 40, no. 6, p. 064301, Jun 2013. [PubMed: 23718620]

[9]. Armstrong I, Kelly M, Williams H and Matthews J, "Impact of point spread function modelling and time of flight on FDG uptake measurements in lung lesions using alternative filtering strategies," EJNMMI Phys, vol. 1, no. 1, p. 99, Dec 2014 [PubMed: 26501457]

[10]. Rahmim A and Tang J, "Noise propagation in resolution modeled PET imaging and its impact on detectability," Phys Med Biol, vol. 58, no. 19, pp. 6945–68, Oct 2013 [PubMed: 24029682]

[11]. van Sluis J, de Jong J, Schaar J, Noordzij W, van Snick P, Dierckx R, Borra R, Willemsen A and Boellaard R, "Performance Characteristics of the Digital Biograph Vision PET/CT System," J Nucl Med, vol. 60, no. 7, pp. 1031–1036, Jul 2019. [PubMed: 30630944]

[12]. Rousset O, Rahmim A, Alavi A and Zaidi H, "Partial Volume Correction Strategies in PET," PET Clin, vol. 2, no. 2, pp. 235–49, 2007 [PubMed: 27157875]

[13]. Epley W, Jacene H, Lodge M and Wahl R, "The impact of PET pixel size on contrast recovery for small lesions," J Nucl Med, vol. 50, no. supplement 2, p. 2018, 2009

[14]. Koopman D, van Dalen J, Lagerweij M, Arkies H, de Boer J, Oostdijk A, Slump C and Jager P, "Improving the detection of small lesions using a state-of-the-art time-of-flight PET/CT system and small-voxel reconstructions," J Nucl Med Technol, vol. 43, no. 1, pp. 21–7, Mar 2015. [PubMed: 25613334]

[15]. Mansor S, Pfaehler E, Heijtel D, Lodge M, Boellaard R and Yaqub M, "Impact of PET/CT system, reconstruction protocol, data analysis method, and repositioning on PET/CT precision: An experimental evaluation using an oncology and brain phantom," Med Phys, vol. 44, no. 12, pp. 6413–6424, Dec 2017. [PubMed: 28994465]

[16]. Rausch I, Ruiz A, Valverde-Pascual I, Cal-González J, Beyer T and Carrio I, "Performance Evaluation of the Vereos PET/CT System According to the NEMA NU2–2012 Standard," J Nucl Med, vol. 60, no. 4, pp. 561–567, Apr 2019 [PubMed: 30361382]

[17]. Rausch I, Cal-González J, Dapra D, Gallowitsch H, Lind P, Beyer T and Minear G, "Performance evaluation of the Biograph mCT Flow PET/CT system according to the NEMA NU2–2012 standard," EJNMMI Phys, vol. 2, no. 1, p. 26, Dec 2015. [PubMed: 26501827]

[18]. Jakoby B, Bercier Y, Conti M, Casey M, Bendriem B and Townsend D, "Physical and clinical performance of the mCT time-of-flight PET/CT scanner," Phys Med Biol, vol. 56, no. 8, pp. 2375–89, 21 Apr 2011 [PubMed: 21427485]

[19]. Rausch I, Mannheim J, Kupferschläger J, la Fougère C and Schmidt F, “Image quality assessment along the one metre axial field-of-view of the total-body Biograph Vision Quadra PET/CT system for 18F-FDG,” EJNMMI Phys, vol. 9, no. 1, p. 87, Dec 2022 [PubMed: 36513949]

[20]. Badawi R, Shi H, Hu P, Chen S, Xu T, Price P, Ding Y, Spencer B, Nardo L, Liu W, Bao J, Jones T, Li H and Cherry S, “First Human Imaging Studies with the EXPLORER Total-Body PET Scanner,” J Nucl Med, vol. 60, no. 3, pp. 299–303, 2019. [PubMed: 30733314]

[21]. NEMA standards publication NU 2–2001 – performance measurements of positron emission tomographs (PET), National Electrical Manufacturers Association, 2001

[22]. Leung E, Revilla E, Spencer B, Xie Z, Zhang X, Omidvari N, Badawi R, Cherry S, Lu Y and Berg E, “A quantitative image reconstruction platform with integrated motion detection for total-body PET,” J Nucl Med, vol. 62, no. supplement 1, p. 1549, May 2021.

[23]. Nardo L, Abdelhafez Y, Spencer B and Badawi R, “Clinical Implementation of Total-Body PET/CT at University of California, Davis,” PET Clin, vol. 16, no. 1, pp. 1–7, Jan 2021 [PubMed: 33218600]

[24]. Razifar P, Sandström M, Schnieder H, Långström B, Maripuu E, Bengtsson E and Bergström M, “Noise correlation in PET, CT, SPECT and PET/CT data evaluated using autocorrelation function: a phantom study on data, reconstructed using FBP and OSEM,” BMC Med Imaging, vol. 5, no. 1, p. 5, 2005. [PubMed: 16122383]

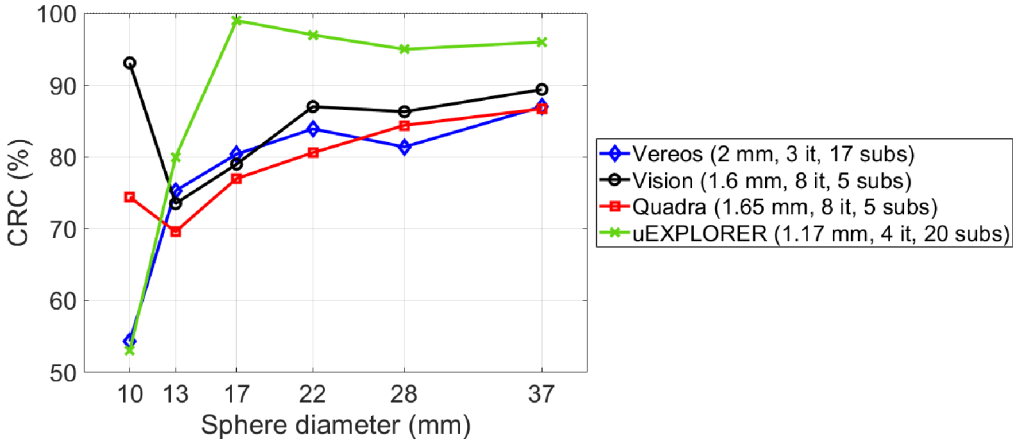

Figure 1.

CRC of four clinical PET/CT scanners: Vereos [16], Digital Biograph Vision [11], Biograph Vision Quadra [5] and uEXPLORER [4].

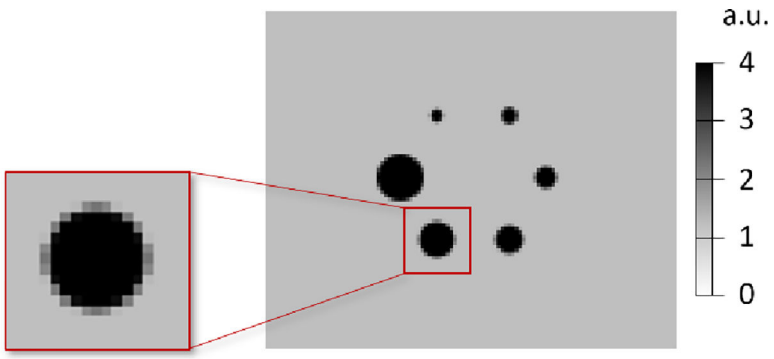

Figure 2.

Example of the central slice from a computer-generated 3D noise-free image using an isotropic voxel size of 2.85 mm and sphere-to-background activity concentration ratio of 4:1. A zoomed version of the 28-mm sphere illustrates the partial voxel filling. Arbitrary units (a.u.) were used.

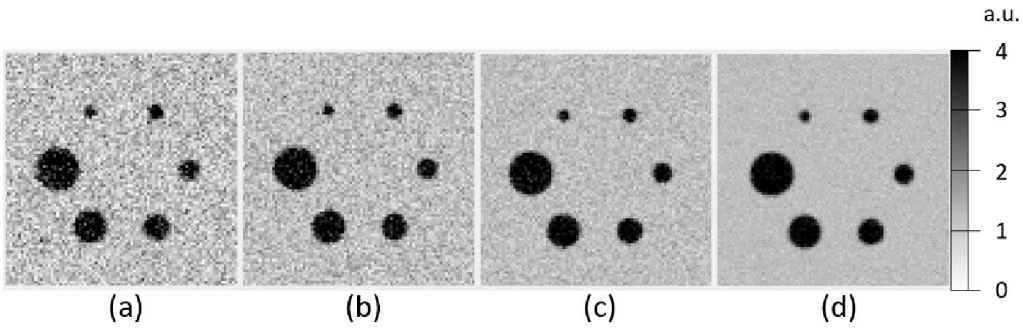

Figure 3.

Examples of computer-generated images with different levels of Poisson noise. From left to right ((a) to (d)), the images have a CV of 44.6%, 31.6%, 19.7%, and 10.0% resulting from an image scaling factor of 5, 10, 25, and 100, respectively.

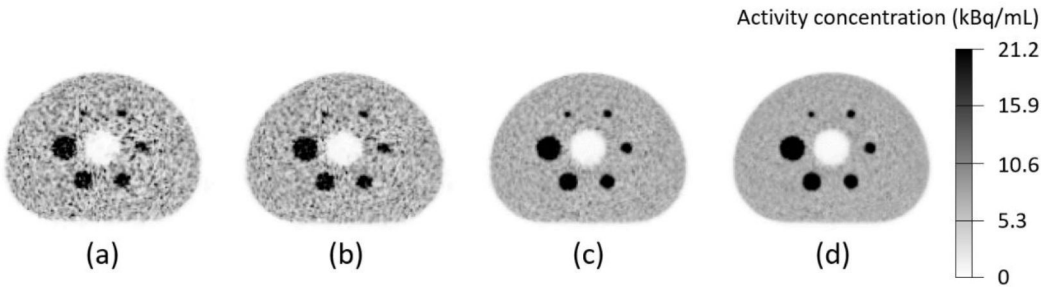

Figure 4.

Reconstructed images of four examples of subsampled datasets generated from a 30-min scan of the NEMA NU2 IQ phantom on the uEXPLORER. From left to right ((a) to (d)), the subsample ratios (SR) were 1/90, 1/60, 1/15 and 1/6, representing virtual frame lengths of 20 s, 30 s, 120 s, and 300 s, resulting in CVs of 44.5%, 36.3%, 18.2%, and 11.8%, respectively.

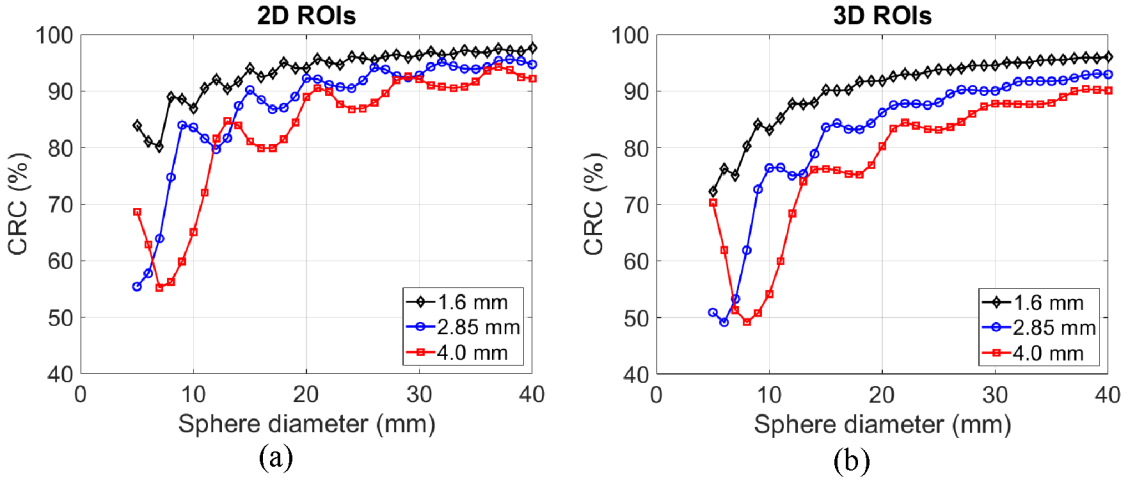

Figure 5.

CRC values obtained with 2D ROIs (a) according to NEMA NU 2 protocol and 3D spherical ROIs (b) for sphere sizes in the range of 5 mm to 40 mm, using three different voxel sizes of 1.6 mm, 2.85 mm, and 4.0 mm.

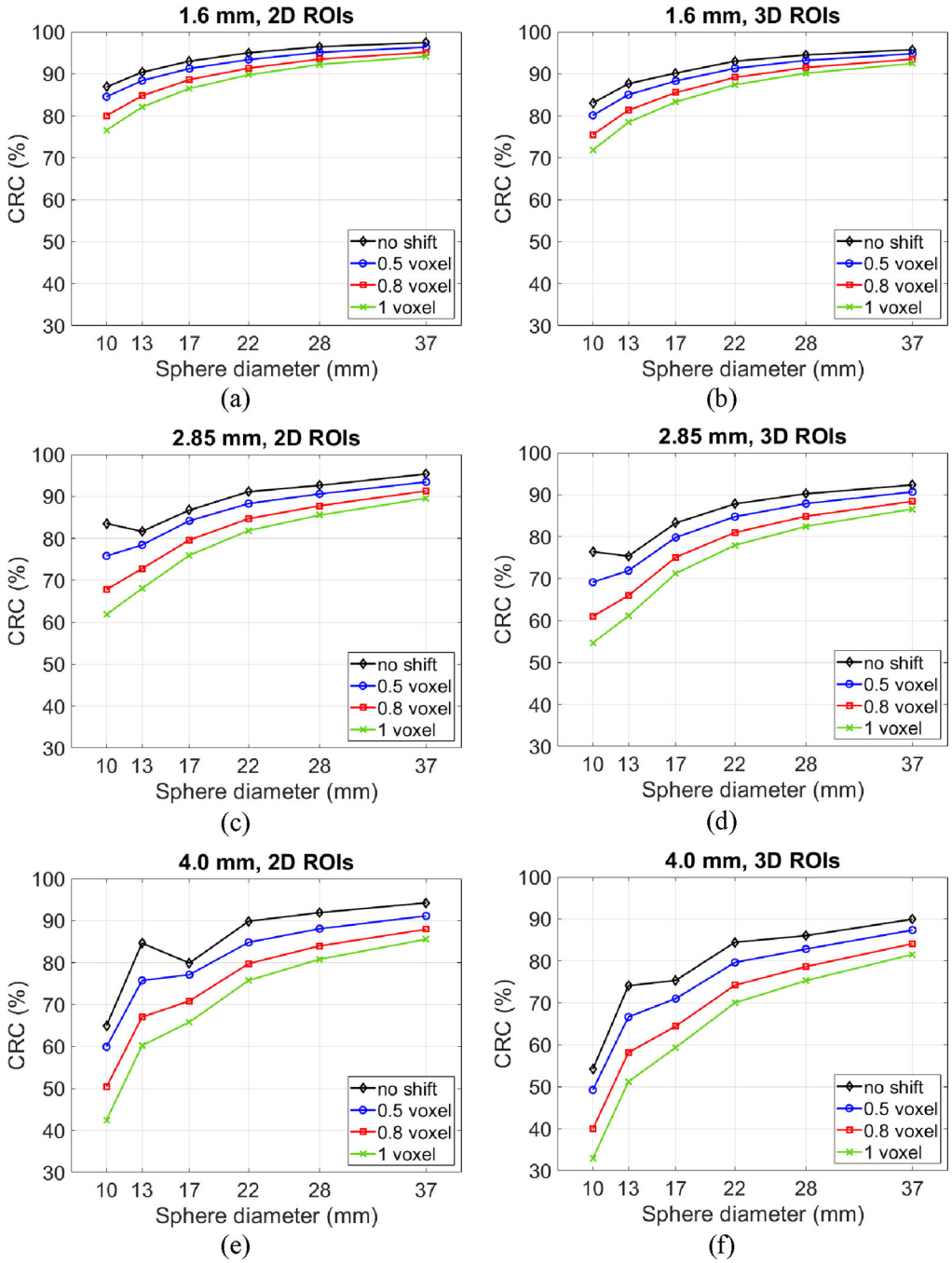

Figure 6.

CRC measurements obtained for the six sphere sizes of the NEMA NU 2 IQ phantom when 2D ROIs ((a), (c), (e)) and 3D ROIs ((b), (d), (f)) are shifted up to one voxel, using three isotropic voxel sizes of 1.6 mm ((a), (b)), 2.85 mm ((c), (d)), and 4.0 mm ((e), (f)).

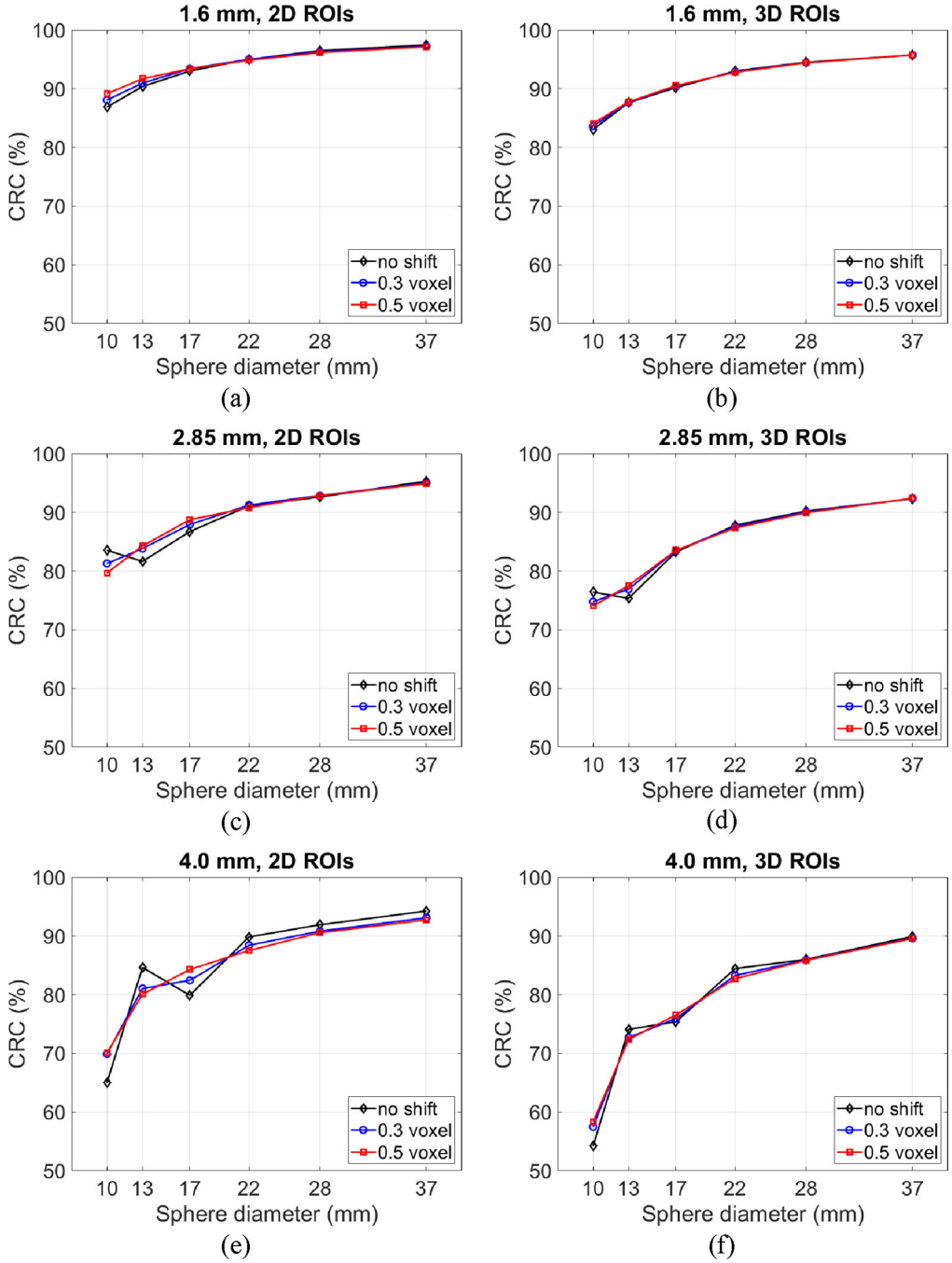

Figure 7.

CRC measurements obtained for the six sphere sizes of the NEMA NU 2 IQ phantom when 2D ROIs ((a), (c), (e)) and 3D ROIs ((b), (d), (f)) are used and sphere position is shifted from the center of the voxel up to half a voxel, using three isotropic voxel sizes of 1.6 mm ((a), (b)), 2.85 mm ((c), (d)), and 4.0 mm ((e), (f)).

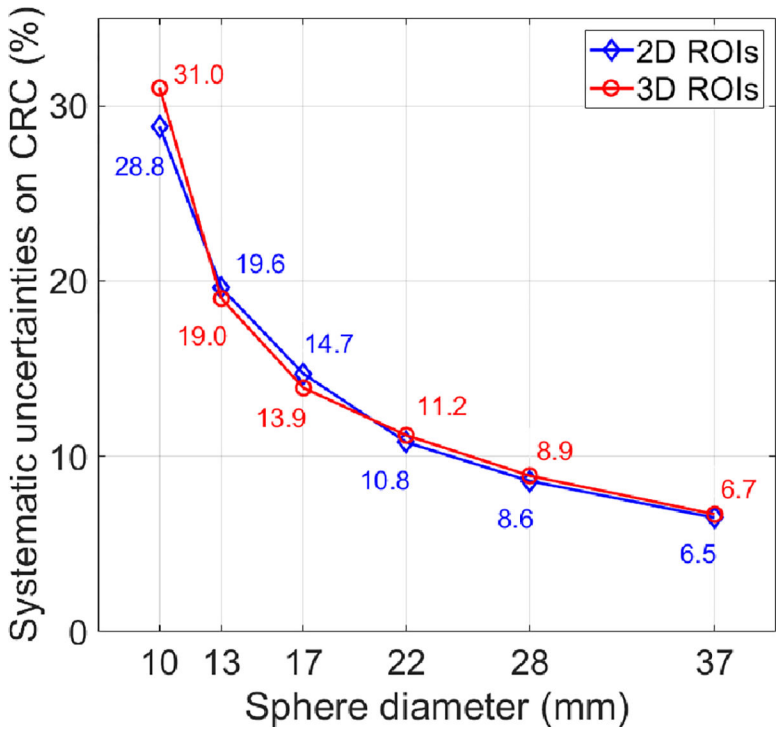

Figure 8.

Systematic uncertainties of the CRC measurement, originating from variations in voxel size, ROI misplacement, and different sphere positions with respect to the image grid.

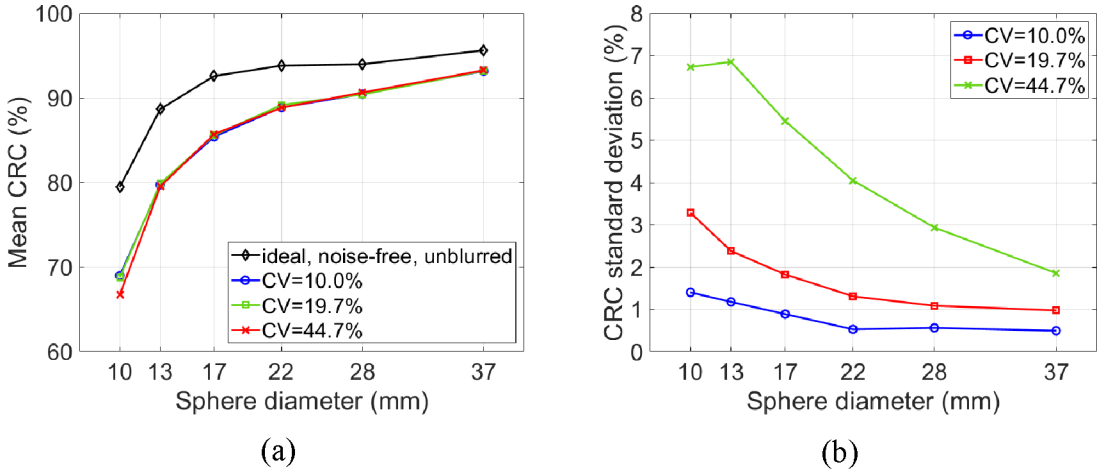

Figure 9.

Mean (a) and standard deviation (b) of the CRC measured on 30 noisy realizations of the computer-generated NEMA IQ images including Poisson noise and 3-mm Gaussian blurring. Images with 3 different noise levels, quantified using CV, are compared to an ideal noise-free image without Gaussian blurring. An isotropic voxel size of 2.344 mm was used in all cases.

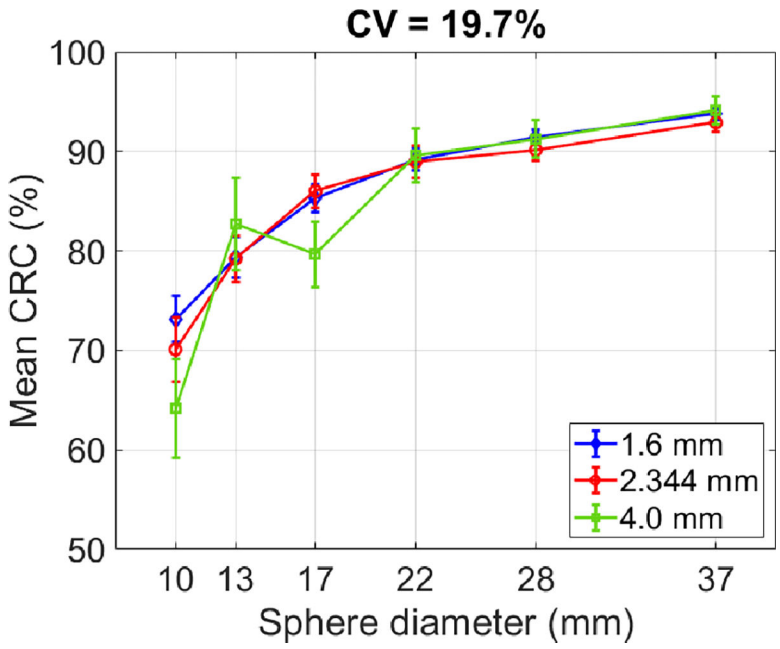

Figure 10.

Mean CRC measured with 2D ROIs on 30 noisy realizations of computer-generated NEMA IQ images including Poisson noise and 3-mm Gaussian blurring using three different voxel sizes. Errors indicate the standard deviation of the CRC measurements for each sphere diameter.

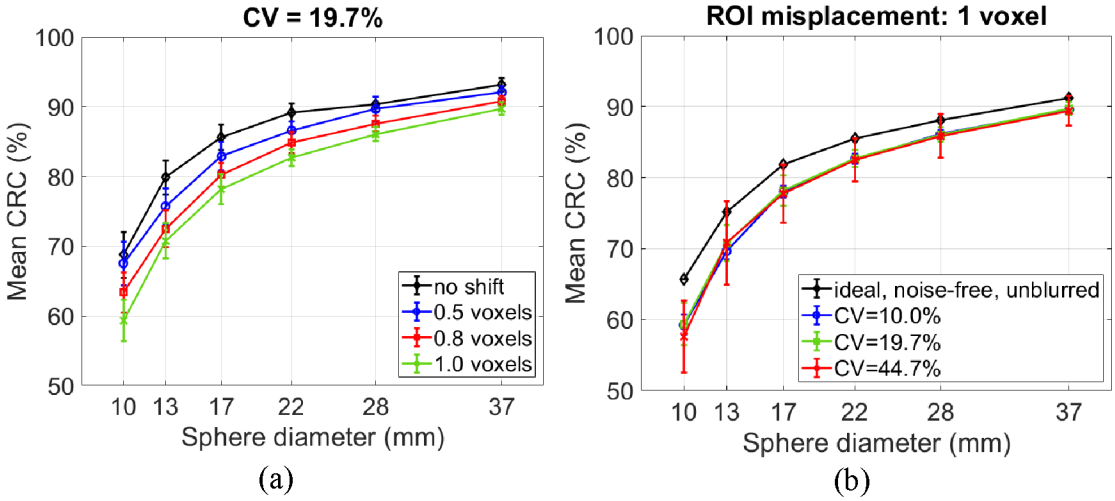

Figure 11.

(a) Effect of ROI misplacement on mean CRC measured on 30 noisy realizations of the computer-generated NEMA IQ images with a CV of 19.7% and ROI misplacements of up to 1.0 voxels. (b) Effect of one-voxel ROI misalignment on the mean CRC values of the image generated with 3 different noise levels, with corresponding CV values between 10.0% and 44.7%. The error bars indicate the standard deviation of the CRC measurement from all realizations for each sphere size and ROI misplacement.

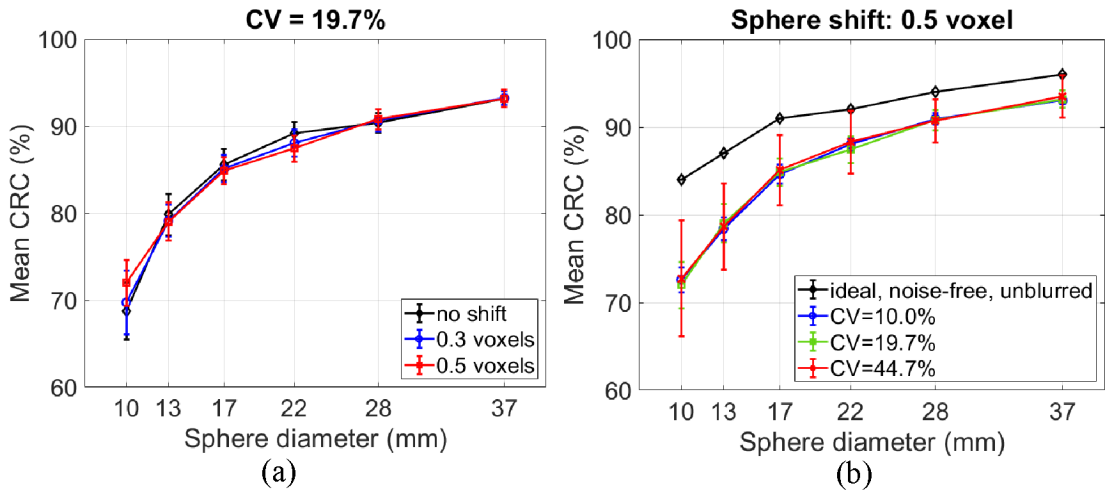

Figure 12.

(a) Effect of sphere position on the image grid on mean CRC measured on 30 noisy realizations of the computer-generated NEMA IQ images with a CV of 19.7% compared for sphere position shifts of up to half a voxel. (b) Effect of a sphere position shift by half a voxel on the mean CRC values measured on 30 noisy realizations of the NEMA IQ image generated with three different noise levels with corresponding CV values between 10.0% and 44.7%. The error bars indicate the standard deviation of the CRC measurement from all realizations for each sphere size and sphere shift.

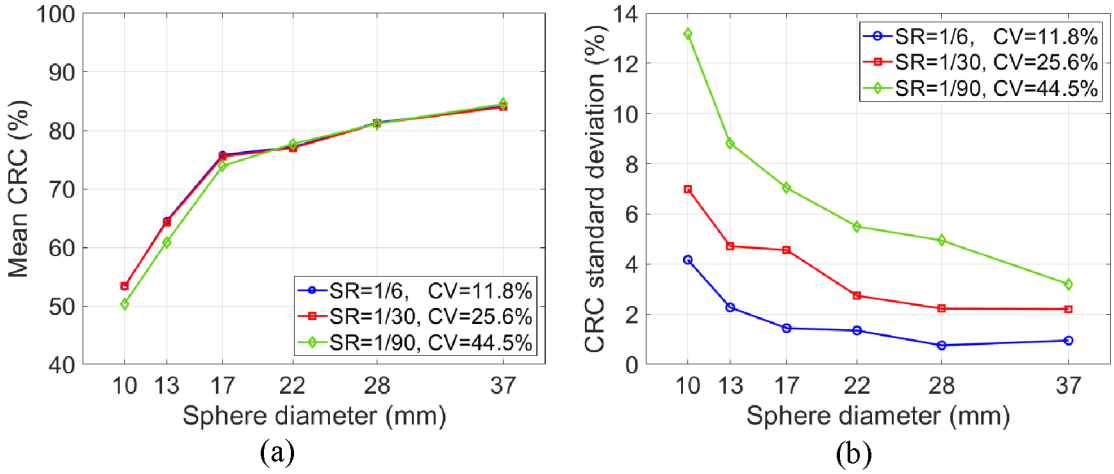

Figure 13.

Mean (a) and standard deviation (b) of the CRC measurements performed on multiple realizations of the uEXPLORER images of the NEMA IQ phantom, subsampled at various noise levels with subsampling rates (SR) corresponding to CV values of 11.8%, 25.6%, and 44.5%.

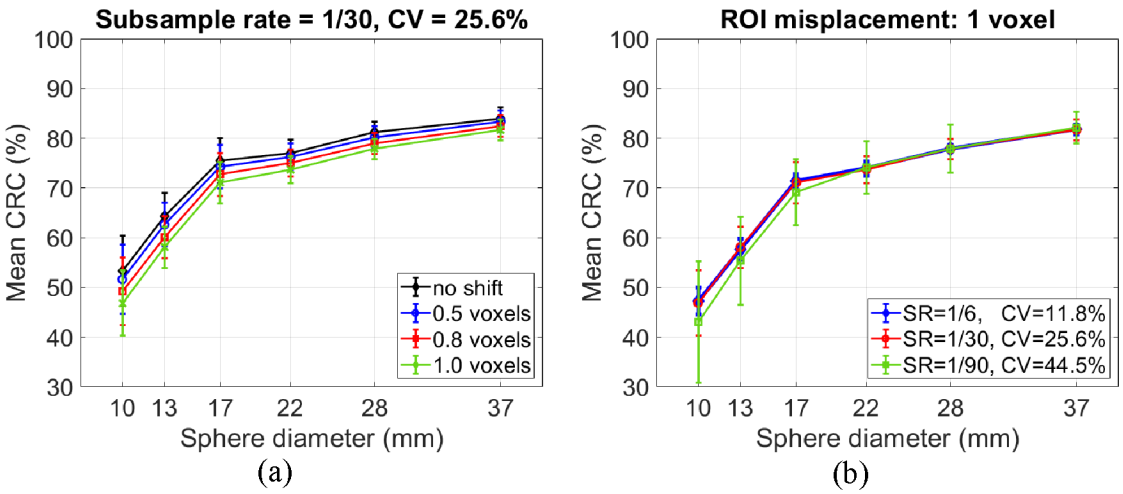

Figure 14.

(a) Effect of ROI misplacement up to one voxel on mean CRC measured on multiple realizations of the uEXPLORER images of the NEMA IQ phantom, subsampled to a CV of 25.6% using a subsampling rate (SR) of 1/30. (b) Effect of one-voxel ROI misalignment on the mean CRC values measured on multiple realizations of the uEXPLORER images of the NEMA IQ phantom, subsampled to three different noise levels, with corresponding CV values between 11.8% and 44.5%. The error bars indicate the standard deviation of the CRC measurement from all realizations for each sphere size and ROI misplacement.

Table 1.

Range and default values of the parameters investigated as sources of systematic uncertainty on the CRC measurement.

Parameter	Range	Default value
Voxel size (mm)	1.0 – 4.0	2.85
ROI misplacement (voxels)	0.0 – 1.0	0.0
Sphere position offset (voxels)	0.0 – 0.5	0.0

Table 2.

Image scaling factors and the resulting CV of computer-generated images with Poisson noise.

Image scaling factor	Coefficient of variation (%)
5	44.7
10	31.6
25	19.7
50	14.1
100	10.0

Table 3.

Overview of all experimental subsampled datasets generated with different subsampling ratios from a 30-min scan of the NEMA NU2 IQ phantom on the uEXPLORER, resulting in different noise levels quantified by CV.

Coefficient of Variation (%)	Subsample ratio	Virtual frame length (s)	Number of realizations
11.8	1/6	300	6
15.0	1/10	180	10
18.2	1/15	120	15
25.6	1/30	60	30
36.3	1/60	30	30
44.5	1/90	20	30
63.0	1/180	10	30